Revealing How Color Vision Phenotype and Genotype Manifest in Individual Cone Cells

Furu Zhang,[1,3] Kazuhiro Kurokawa,[1] Marcel T. Bernucci,[1] Hae Won Jung,[1] Ayoub Lassoued,[1] James A. Crowell,[1] Jay Neitz,[2] Maureen Neitz,[2] and Donald T. Miller[1]

[1]School of Optometry, Indiana University, Bloomington, Indiana, United States
[2]Department of Ophthalmology, University of Washington, Seattle, Washington, United States
[3]Center for Devices and Radiological Health, Food and Drug Administration, Silver Spring, Maryland, United States

Correspondence: Furu Zhang, School of Optometry, Indiana University, 800 E. Atwater Avenue, Bloomington, IN 47405, USA; furzhang@iu.edu.

Received: October 14, 2020
Accepted: January 15, 2021
Published: February 5, 2021

Citation: Zhang F, Kurokawa K, Bernucci MT, et al. Revealing how color vision phenotype and genotype manifest in individual cone cells. *Invest Ophthalmol Vis Sci.* 2021;62(2):8. https://doi.org/10.1167/iovs.62.2.8

Purpose. Psychophysical and genetic testing provide substantial information about color vision phenotype and genotype. However, neither reveals how color vision phenotypes and genotypes manifest themselves in individual cones, where color vision and its anomalies are thought to originate. Here, we use adaptive-optics phase-sensitive optical coherence tomography (AO-PSOCT) to investigate these relationships.

Methods. We used AO-PSOCT to measure cone function—optical response to light stimulation—in each of 16 human subjects with different phenotypes and genotypes of color vision (five color-normal, three deuteranopic, two protanopic, and six deuteranomalous trichromatic subjects). We classified three spectral types of cones (S, M, and L), and we measured cone structure—namely cone density, cone mosaic arrangement, and spatial arrangement of cone types.

Results. For the different phenotypes, our cone function results show that (1) color normals possess S, M, and L cones; (2) deuteranopes are missing M cones but are normal otherwise; (3) protanopes are missing L cones but are normal otherwise; and (4) deuteranomalous trichromats are missing M cones but contain evidence of at least two subtypes of L cones. Cone function was consistent with the subjects' genotype in which only the first two M and L genes in the gene array are expressed and was correlated with the estimated spectral separation between photopigments, including in the deuteranomalous trichromats. The L/M cone ratio was highly variable in the color normals. No association was found between cone density and the genotypes and phenotypes investigated, and the cone mosaic arrangement was altered in the dichromats.

Conclusions. AO-PSOCT is a novel method for assessing color vision phenotype and genotype in single cone cells.

Keywords: adaptive optics, functional imaging, color vision, optical coherence tomography, genetics of color vision

Trichromatic human color vision is realized by mixing neural signals from cone photoreceptors containing three types of photopigments that are sensitive to long (L-cone), medium (M-cone), and short (S-cone) wavelengths of light. Absence or dysfunction of any type is known to cause color vision loss and affects many: 0.8% to 7.4% of males and 0.03% to 0.6% of females, depending on race.[1] Color vision performance is routinely assessed psychophysically by matching or discriminating colors. Genetic testing, which has advanced considerably over the past three decades, elucidates the molecular mechanisms of color vision,[2] thereby augmenting psychophysical testing and providing a more robust clinical diagnosis of color vision deficiencies.[3] Although these methods provide substantial information regarding an individual subject's color vision, information regarding how color vision manifests itself in the response and structure of single cone cells, where color vision and its anomalies originate, remains incomplete.

Microspectrophotometry[4] and suction electrophysiology[5] measure the response of individual cones to light stimuli of different wavelengths (cone spectral sensitivity), but these methods are limited to postmortem measurements, as they destroy the tissue they measure. They have also been reported on small numbers of cones (e.g., 33 cones[4]; seven cones[5]), due to the complexity of the techniques involved and difficulty of preparing the delicate tissue. Measurements in the living human eye using, for example, retinal densitometry[6,7] and electroretinography[8] avoid postmortem artifacts and are conducive to large sample sizes. But, they measure the aggregate response of thousands, if not millions, of photoreceptors and other cells due to insufficient spatial resolution and limited ability to isolate cone responses from those of other cell types.

The development of adaptive optics (AO) to correct ocular aberrations in high-resolution retinal imaging ophthalmoscopes[9] has led to measurements of individual cone reflectance differences in the living human eye,[10]

Table 1. Subject Data Showing Age, Axial Eye Length, Psychophysical Color Testing (HRR, Anomaloscope, and Resulting Clinical Phenotype), and Genetic Testing

Subject					Anomaloscope			
#	ID	Age (y)	Eye Length (mm)	HRR	Match Midpoint	Match Range	Phenotype	Genotype
1	130	22	24.72	Normal	42.4	4.6	Normal	LM (29 nm)
2	168	22	26.35	Normal	42.9	8	Normal	LM (29 nm)
3	116	29	24.00	Normal	42.65	5.1	Normal	LM (29 nm)
4	155	31	24.75	Normal	42.95	3.5	Normal	LM (29 nm)
5	53	52	25.40	Normal	40.65	1.1	Normal	LM (29 nm)
6	177	21	24.35	Strong deutan	36.5	73	Deuteranopia	LM^{C203R} (0 nm)
7	151	24	24.68	Strong deutan	36.5	73	Deuteranopia	L (0 nm)
8	162	24	24.59	Medium deutan	36.5	73	Deuteranopia	L (0 nm)
9	161	24	21.76	Unclassified	36.5	73	Protanopia	M (0 nm)
10	163	37	23.44	Medium protan	36.5	73	Protanopia	M (0 nm)
11	159	22	24.03	Mild deutan	20.6	5.8	Deuteranomalous	LL (6.5 nm)
12	158	22	24.34	Medium deutan	17.75	29.7	Deuteranomalous	LLL (N/A)
13	165	23	24.43	Mild deutan	16.9	5.2	Deuteranomalous	LLM (2.5 nm)
14	122	30	24.34	Medium deutan	11.2	16.6	Deuteranomalous	LL (2.5 nm)
15	157	31	24.05	Medium deutan	15.85	16.9	Deuteranomalous	LLM (2.5 nm)
16	169	51	24.19	Medium deutan	23.6	32.4	Deuteranomalous	LLM (2.5 nm)

The genotype column lists the order of the detected M and L opsin genes in the X-chromosome tandem array at Xq28 and the predicted spectral separation of the first two genes in the array (given in parentheses). The C203R mutation was detected in subject S6, as denoted by M^{C203R}. Not shown are the brightness of the yellow hemifield as measured with the anomaloscope. Subjects S9 and S10 required higher yellow brightness (25.9 and 27.5) to match pure green (0 on red–green mixture axis) and lower yellow brightness (1.9 for both subjects) to match pure red (73 on red–green mixture axis). For the other subjects, the required matching brightness of the yellow hemifield fell within the range of 12.7 to 15.4 (average ± SD, 14.1 ± 0.8), regardless of the mixture ratio of red and green, indicating no luminosity loss at long wavelengths.

bringing the study of color vision to the cellular scale in vivo. The pioneering work of Roorda and Williams[10] combined AO and retinal densitometry to measure photobleach-induced reflectance changes of individual cones. Using this reflectance signal as a biomarker of cone function, they differentiated the three spectral types of cones and mapped the chromatic cone mosaics of subjects with normal and dichromatic color vision. Although their approach was successful, the necessity for high bleach levels by multiple light sources and repeated measurements to attain an adequate signal resulted in long experiments (5 days,[10], 1–3 days,[11] 3–9 hours[12]) and relatively large uncertainties of 3.6% ± 1.6% in classification (average ± SD of uncertainties of 20 measurements from 13 color-normal humans and four monkeys reported in four AO retinal densitometry studies).[10–13] Perhaps because of these shortcomings, AO-enhanced retinal densitometry has been used in a limited number of color vision studies. Using this method, cone photoreceptors have been classified in 13 color-normal subjects and two dichromats, as reported in five publications.[10–14]

Recently developed AO phase-sensitive optical coherence tomography (AO-PSOCT) by our laboratory[15] and others[16–18] resolves individual cone cells in three dimensions and measures their functional response to brief flashes of light with exquisite sensitivity. Different from AO retinal densitometry that relies on reflectance changes of cones to measure function, our AO-PSOCT method uses phase information that is sensitive to optical path length (OPL) changes in the cone outer segment as small as 5 nm.[15] We found that, when cones are stimulated with a short flash of visible light, their outer segments (OSs) exhibit a rapid OPL increase with an amplitude up to a couple hundred nanometers, depending on the wavelength and strength of the light stimulus and the cone spectral type (S, M, or L). Further characterization of this light-induced OPL change has shown that it results from phototransduction of the cone and provides a highly accurate (<0.02% uncertainty) and efficient (5 seconds to 30 minutes to acquire measurements) means for classifying cone types.[15] These advantages make it a potentially useful tool to investigate the role that cone photoreceptors play in color vision.

In this study, we used AO-PSOCT to measure the individual response of many thousands of cones in 16 human subjects with different phenotypes and genotypes of color vision. By comparing these responses, we show how different phenotypes and genotypes are expressed at the level of individual cone cells. Clear differences in cone response were found between all phenotypes examined, including between deuteranopic and deuteranomalous trichromatic subjects. For different genotypes, our results are consistent with expression of the first two genes in the X-chromosome gene array and strongly correlate with the estimated spectral separation between photopigments encoded by these genes.

Method

Subjects

Eleven subjects with red–green color vision deficiency and five color-normal subjects (as determined from psychophysical testing described in the next section) participated in the study (Table 1). Data acquired on three of the subjects (S1, S5, and S8) were reported in our previous publication[15] but re-analyzed in this study. The color-normal subjects were recruited to match the age, gender, and race of the color-deficient subjects. Subjects were all male and had best-corrected visual acuity of 20/20 or better and a spherical equivalent refractive error between 0 and –6 diopters. Eye lengths ranged from 21.76 mm to 26.35 mm (see Table 1) as measured with the IOLMaster (Carl Zeiss Meditec, Jena, Germany) and were used to scale the AO-PSOCT retinal

Investigative Ophthalmology & Visual Science

images from degrees to millimeters.[19] All subjects were free of ocular disease based on a prior eye exam within the last year and further evaluation of the retina with Spectralis OCT (Heidelberg Engineering, Heidelberg, Germany) as part of this study. All procedures on the subjects adhered to the tenets of the Declaration of Helsinki and were approved by the Institutional Review Board of Indiana University. Genetic testing was also approved by University of Washington. Prior to data collection, written informed consent was obtained after the nature and possible risks of the study had been explained.

Psychophysical Testing

We used two different psychophysical tests to determine the color vision phenotypes of the 16 subjects. Subjects were tested first with Ishihara and Hardy–Rand–Rittler (HRR, 4th edition; Good-Lite, Elgin, IL, USA) pseudoisochromatic plates as a pre-assessment of phenotype (normal, deutan, or protan) and severity of color vision deficiency (mild, medium, or strong). Then, more sensitive color matching tasks were administered using the HMC-Anomaloskop (Oculus, Wetzlar, Germany). Phenotype was determined from the matching range and midpoint of the green (549 nm) and red (666 nm) mixture hemifield of the anomaloscope and from the brightness of the yellow (589 nm) reference hemifield. Matching range is a numeric scale (0 for pure green to 73 for pure red), over which the mixture of the red and green hemifield in the anomaloscope appears equal in color to the yellow hemifield to the subject. Matching midpoint is the middle numeric value of the matching range. The brightness is a numeric scale of the yellow hemifield (0 for dim to 45 for bright) that matches the brightness of the mixture hemifield.

Genetic Testing

Saliva samples were collected from all subjects using a DNA collection kit (Oragene Discover OGR-500; DNA Genotek Inc., Ottawa, ON, Canada). The L- and M-cone opsin genes were separately and specifically amplified in the PCR and were used in a second round of PCR to amplify and sequence exons 2, 3, and 4 of the L and M opsin genes, as previously described.[3] The relative number of L versus M opsin genes on the X-chromosome for each subject was estimated via mass spectrometry with the MassArray System (Agena Bioscience, San Diego, CA, USA).[3] The spectral peaks of the L- and M-cone photopigments were estimated based on the effects of encoded amino acid sequences on spectral tuning.[20]

AO-PSOCT Experiment

Indiana AO-PSOCT System. The AO-PSOCT system has been described previously.[15,21,22] Briefly, the system uses a light source with a center wavelength of 790 nm and bandwidth of 42 nm, providing a nominal axial resolution of 4.7 µm in retinal tissue (refraction index of the sample, n = 1.38). The diffraction-limited lateral resolution of 2.4 µm is realized by the AO subsystem, which dynamically measures and corrects the ocular aberration across a 6.7-mm pupil of a subject's eye at a control loop rate up to 123 measurements and corrections per second. The detection arm contains four high-speed spectrometers that are connected to a 1 × 4 fiber-based optical switch. By synchronizing the optical switch and spectrometer exposure durations, the system is scalable to A-line speeds of 250 kHz (one-camera mode), 500 kHz (two-camera mode), and 1 MHz (four-camera mode). In this study, we used the 1-MHz four-camera mode operation in order to optimize tracking of the light-stimulated cone dynamics.

Three fiber-based light-emitting diode (LED) sources (LEDMOD455, LEDMOD528, and LEDMOD625; Omicron-Laserage Laserprodukte GmbH, Rodgau, Germany) with spectra of 450 ± 8 nm, 528 ± 12 nm, and 637 ± 12 nm (maximum ± half-width at half-maximum), respectively, were used to stimulate cone photoreceptors. These three wavelength bands were selected because they cover a wide range of absorption efficiencies of the three cone types. Spectral sensitivities of the three cone types to the 450-nm, 528-nm, and 637-nm stimuli obey the ordinal relations S > M > L, M > L > S, and L > M > S, respectively, as shown previously.[15]

Lights of the three sources were combined and co-aligned with the AO-OCT imaging beam using dichroic beam splitters. The stimuli formed a 6-mm beam at the eye pupil and illuminated a 2°-diameter circular retinal patch concentric to the AO-OCT beam. We controlled the timing and power level of the LEDs with a function generator (Agilent 33220A; Agilent Technologies, Santa Clara, CA, USA) that was triggered by an open-source Arduino microcontroller. The microcontroller placed the trigger at a preset time in the video acquisition by monitoring the start of each AO-OCT volume acquisition, which occurred every 100 ms. Timing uncertainty of the LED flash onset was ±0.6 ms (±SD) relative to the start of the AO-OCT volume acquisition. Rise and fall times of the LED flashes were 4 µs (10% to 90% of the steady value of the flash), producing a pristine top-hat profile.

The combined energy entering the eye of the AO-OCT beam (<430 µW) and light stimulation flash (95–320 µW, depending on source) was within safe limits established by the American National Standards Institute.[23]

AO-PSOCT Imaging. The eye to be imaged was dilated with one drop of 1% tropicamide prior to AO-OCT imaging. AO-OCT volume videos (0.8° × 1°) were collected at 3.7° temporal retina of all subjects with a lateral sampling of 1 µm/pixel and an A-line rate of 1,000,000 lines/s. Volumes were acquired at 10 Hz over a 5-second duration. At 2.5 seconds, a 5-ms flash of visible light was delivered to the retina. The power levels used to stimulate retina for each wavelength band were 200 µW (450 nm), 95 µW (528 nm), and 330 µW (637 nm), which were estimated to bleach 1.1%, 9.9%, and 8.7% of the collective L and M photopigment, respectively, as described by Rushton and Henry.[24] For each stimulus wavelength, we acquired 15 videos in order to improve SNR by averaging. Between videos, there was an empirically determined 90 seconds of dark adaption to prevent influence from preceding videos, resulting in a total image acquisition time of 30 minutes for each stimulus and 90 minutes for the entire experiment.

Data Processing and Analysis. After data collection, the optical signature of cone function—temporal change in the OPL of the OS of the cone—was extracted from each cone using the method described previously.[15] In brief, we first computed the phase difference (φ_{OS}) between the inner segment/outer segment junction and cone OS tip reflections of each cone, and then we computed cone response traces given as the phase difference ($\Delta\varphi_{OS}$) between the phase of the cone in each volume and pre-stimulus volume

Investigative Ophthalmology & Visual Science

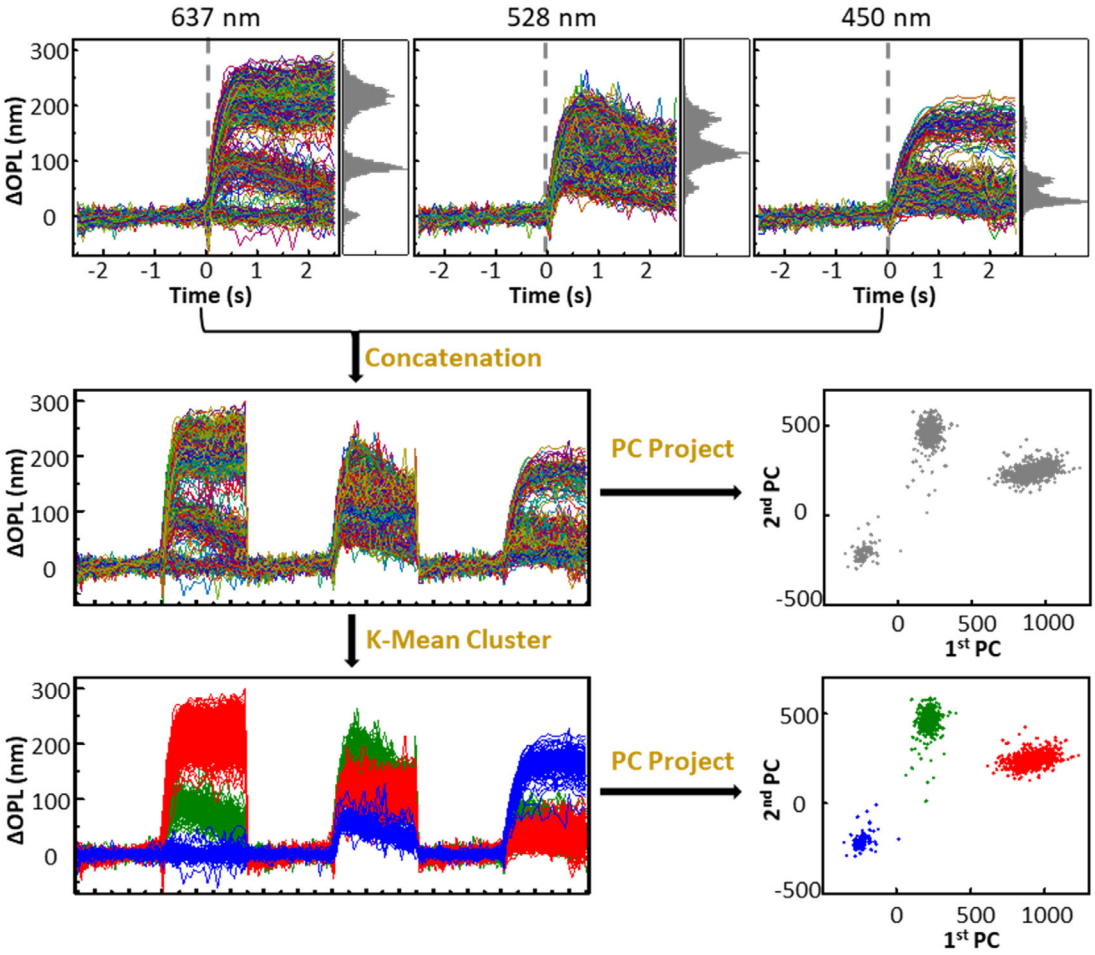

Figure 1. Procedure for processing AO-PSOCT cone response traces. (*First row*) Measured responses of 1300 cones in a color-normal subject (S3) after stimulation by a brief flash from one of three spectral sources: 637 nm, 528 nm, or 450 nm. Individual cone traces are randomly colored; the *gray vertical dashed line* at 0 seconds represents the 5-ms stimulus. (*Second row*) The left graph concatenates the three responses in the top row. Each concatenated trace is a single cone, and its first two principal components are plotted in the right graph. Each trace corresponds to one point in the plot. (*Third row*) Copy of the second row but with cones classified as L cones (*red*), M cones (*green*), and S cones (*blue*), based on *k*-mean cluster analysis.

of the same video. Thus, each video generated a single, one-dimensional response trace for each cone consisting of 50 measurements (one per volume) spaced every 0.1 second. To improve the signal-to-noise ratio, traces were averaged over the 15 videos (i.e., average of the complex OCT signal, which contains both amplitude and phase), then converted to phase ($\overline{\Delta\varphi_{OS}}$), unwrapped if necessary, and finally converted to optical path length difference (ΔOPL) as given by $\overline{\Delta\varphi_{OS}}\,\frac{\lambda}{4\pi}$, where λ is the center wavelength of the AO-OCT system.

Figure 1 depicts our analysis of the cone ΔOPL traces, illustrated with one of the color-normal subjects (subject S3). The first row shows time traces of the cone responses (ΔOPL) to flash stimulation by the three LEDs. We concatenated the three responses associated with each cone (middle row, left) to facilitate analysis by principal component analysis (PCA).[25] The combined traces extended across 150 dimensions (3 × 50 measurements per cone). We used PCA to reduce the 150 dimensions to two dimensions, corresponding to the first two principal components and capturing most of the trace variance (see below). We refer to this plot (middle row, right side) as being in the PC space. Finally, we determined the number of cone groups in the PC space (based on visual appearance of clusters), grouped them with a *k*-mean cluster algorithm,[26] and assigned cone groups to spectral classes on the basis of expected spectral sensitivities to each stimulus wavelength. Classification results for the color-normal subject are shown color coded in the third row of Figure 1.

We observed that different subjects had slightly different PC spaces (i.e., different principal components), as the PC space is determined by the unique cone traces of each subject. This difference complicates intersubject comparison. To address this, we projected the trace responses of all subjects to the same PC space, which we arbitrarily selected as the PC space of subject S3. Although this projection technically only captures the maximum variance for subject S3, the difference for our other subjects was found to be small, a finding not unexpected given the similar response of their cones. Our analysis revealed that projection of all subjects to the PC space of subject S3 captured, on average, 81.5% ± 8.8% of their variance in the first two PC dimensions, which is only 6.3% smaller than projecting to each subject's unique PC space (87.8% ± 5.8%). Because of the small difference,

Investigative Ophthalmology & Visual Science

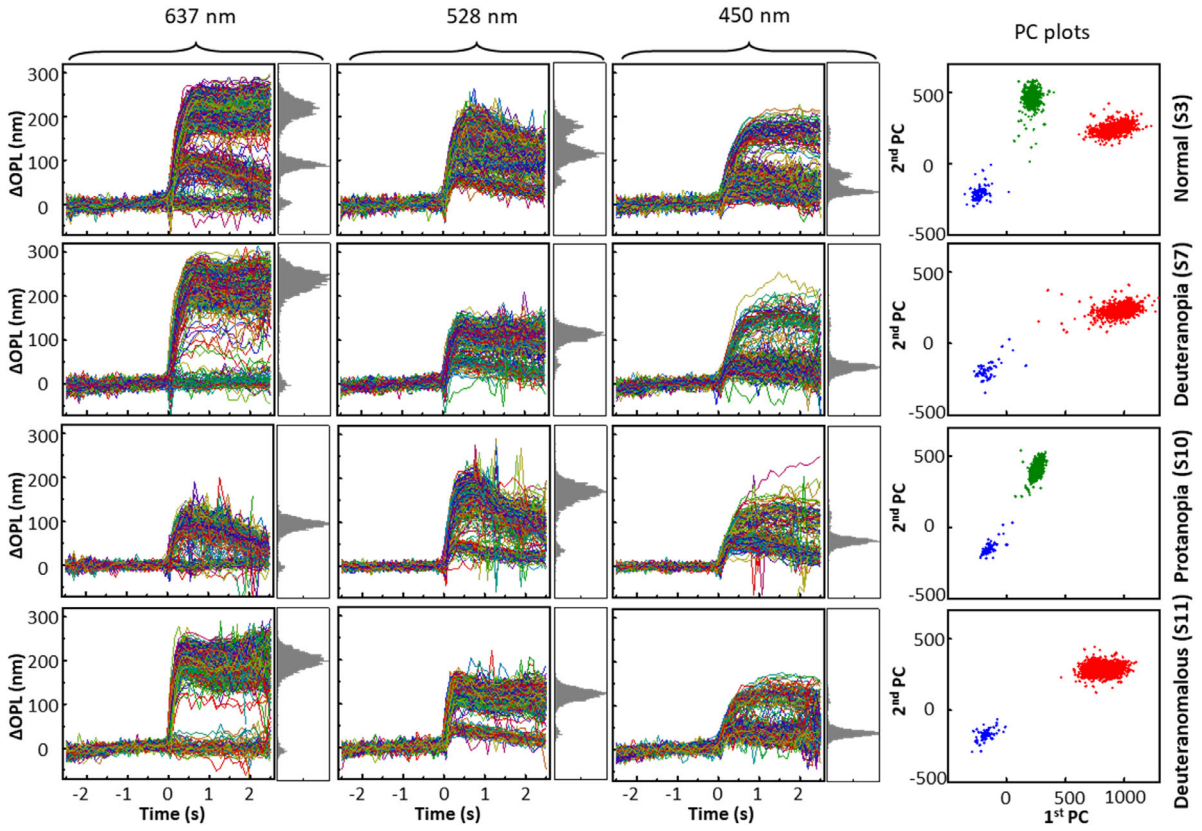

Figure 2. AO-OCT cone results of four representative subjects of different phenotypes: color-normal (*first row*), deuteranope (*second row*), protanope (*third row*), and deuteranomalous trichromats (*fourth row*). The first three columns show cone responses to the three stimuli: 637 nm (*first column*), 528 nm (*second column*), and 450 nm (*third column*). Histograms of normalized cone counts are shown for 0.5 to 1 second after stimulus onset. The *fourth column* shows the cone traces transformed into the PC space and color coded by identified spectral type: *red* (L cone), *green* (M cone), and *blue* (S cone).

all subject data are shown in the PC space of subject S3, and to simplify terminology the term PC space refers only to that of subject S3, regardless of subject.

In addition to the above analysis of the cone ΔOPL traces and their representation in PCA space, we also analyzed the skewness of the cone clusters in PCA space to detect cone subtypes. A description of this analysis is given in the Results section, as it is best understood in the context of the results. We also extracted several biomarkers of cone structure from the AO-OCT volume images. These included cone density that was measured using a semi-automatic detection method, arrangement of the cone mosaic (specifically, number of nearest cone neighbors) using Voronoi analysis, missing cones by visual inspection of the cone mosaic for dark holes, proportion of each type of cone (S, M, and L), and, finally, reconstruction of the chromatic cone mosaic using our S, M, and L classification.

Results

Psychophysical and Genetic Testing

Table 1 summarizes the phenotype and genotype of the 16 subjects. Phenotype was obtained with the HRR pseudoisochromatic plates and the anomaloscope, and the genotype was obtained with the MassArray System.[3]

Subjects S1 to S5 were determined to be normal trichromats. The subjects performed as normal on the HRR and within the normal range of the anomaloscope color-matching midpoint, matching range, and brightness of the yellow hemifield. Subjects S6 to S10 demonstrated dichromatic behavior. Four of the five performed as deutan or protan on the HRR. As expected of dichromats, the subjects matched any mixture of red and green light with the yellow reference light in the anomaloscope test. Combining this lack of green–red discrimination with the flat (S6–S8) and skewed (S9 and S10) brightness of the yellow hemifield measurements (described in Table 1 caption), subjects S6 to S8 were determined to be deuteranopes and subjects S9 and S10 protanopes.

Subjects S11 to S16 were diagnosed as anomalous trichromats. The six performed as either mild or medium deutan on the HRR. Their color-matching midpoints and range, as measured with the anomaloscope, were shifted toward the green light (545 nm), indicating their clinical phenotype as deuteranomalous trichromats. Among subjects S11 to S16, high intersubject variability of color-matching performance was observed, with the color-matching range varying from 5.2 to 32.4 (average ± SD, 17.8 ± 11.5).

As shown in Table 1, the genotypes of the five color-normal subjects all showed one L gene followed by one M gene in the X-chromosome tandem array at location Xq28. Separation of the spectral absorption peaks of the L and M genes was estimated to be 29 nm. The three deuteranopes (subjects S6–S8) carried a single L gene. Subjects S7 and S8 carried no M gene, and subject S6 carried one M gene

Investigative Ophthalmology & Visual Science

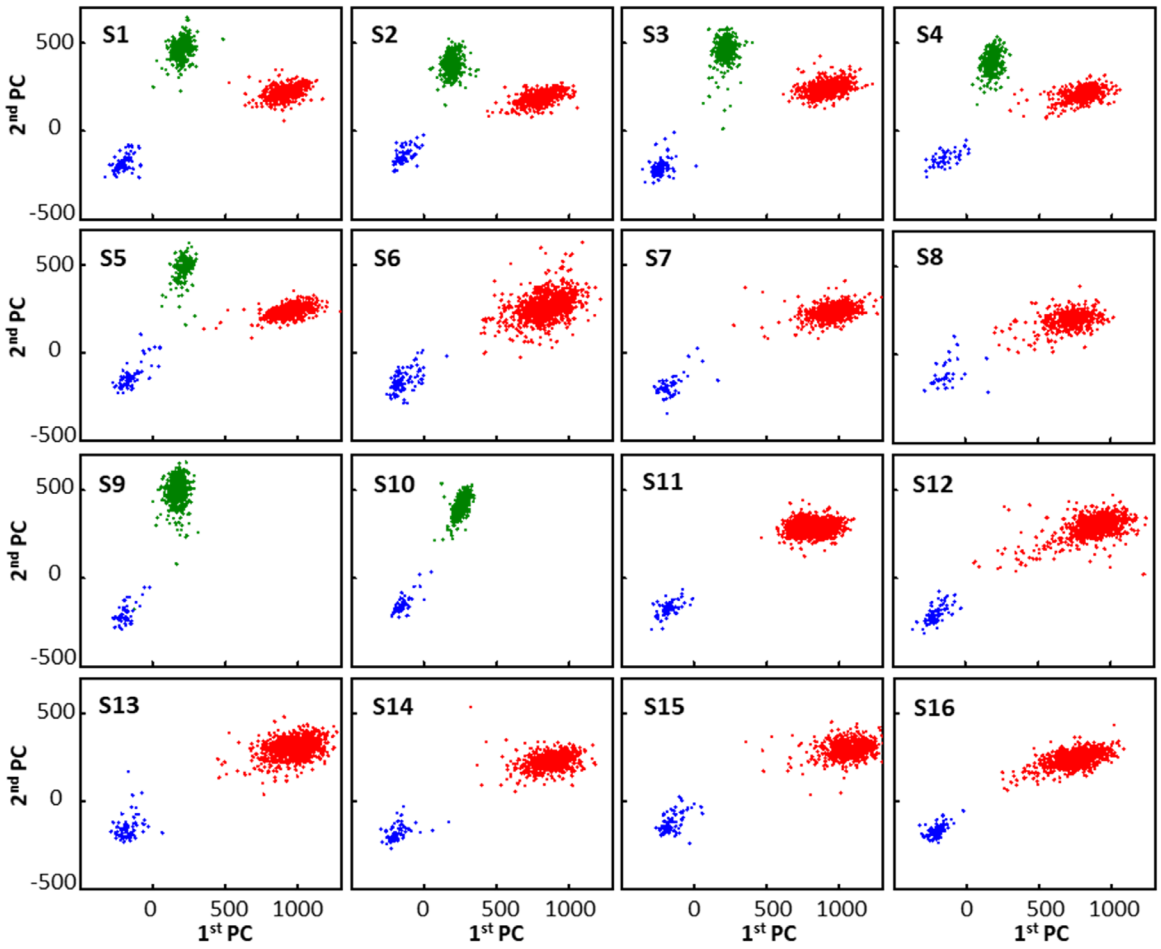

Figure 3. Cone response in the PC space of the 16 subjects in this study. Cones are color coded by spectral type: *red* (L cone), *green* (M cone), and *blue* (S cone). Subjects are grouped by phenotype: color-normal, S1–S5; deuteranope, S6–S8; protanope, S9 and S10; and deuteranomalous trichromats, S11–S16. The number of cones per plot ranged from 587 to 1469 (average ± SD, 1063 ± 221); the lowest cone number (587) was found in subject S8 because of his notably larger eye motion during imaging.

with C203R mutation that was distal to the L gene. Both protanopes (subjects S9 and S10) carried a single M gene and no L gene.

The deuteranomalous trichromats (subjects S11 to S16) exhibited remarkable genetic diversity, both in terms of number of opsin genes in the gene array and the estimated spectral separation between the opsins encoded by the first two heterozygous L genes. Five deuteranomalous trichromats carried two L genes encoding spectrally different photopigments. S12 carried three L genes. Subjects S13, S15, and S16 also carried an M gene that was located distal to the two L genes. The spectral separation between photopigments encoded by the first two heterozygous L genes was estimated as 6.5 nm in subject S11 and 2.5 nm in subjects S13 to S16. An estimate was not made for subject S12 because the ordering of his three L genes was unknown. Each order can produce different active combinations with different spectral separations.

Cone Response by Phenotype

We successfully measured the response (ΔOPL) of thousands of cones to three different spectral stimuli in each subject. Cone function was significantly different between subjects of different color vision phenotype. To illustrate, Figure 2 shows the response of approximately 1000 cones in each of four subjects representing a different phenotype. The three leftmost columns of Figure 2 plot the temporal response of cones after a single flash of 637 nm, 528 nm, or 450 nm stimulus. The cone traces transformed to the PC space are displayed in the fourth column. Results in the PC space for all 16 subjects are displayed in Figure 3.

For the five color-normal subjects (subjects S1–S5), the cone responses formed a trimodal distribution, with each mode corresponding to one of the three spectral types of cones. Cone type appeared to be better separated in the PC space (three clusters), which was expected as the first two principal components capture the majority of the variance across cone responses for all three stimuli.

For the three deuteranopes (subjects S6–S8), we observed only two types of cone responses in the trace distribution (bimodal) and PC space (two clusters). These followed what would be expected of L and S cones as observed in the five normal subjects. Neither followed what was expected of M cones; for example, the M cluster in the PC space of normal subjects was absent in the deuteranopes (Fig. 3, PC space plots for subjects S6–S8). The same pattern was observed in the two protanopes (subjects S9 and S10), but with cone

Investigative Ophthalmology & Visual Science

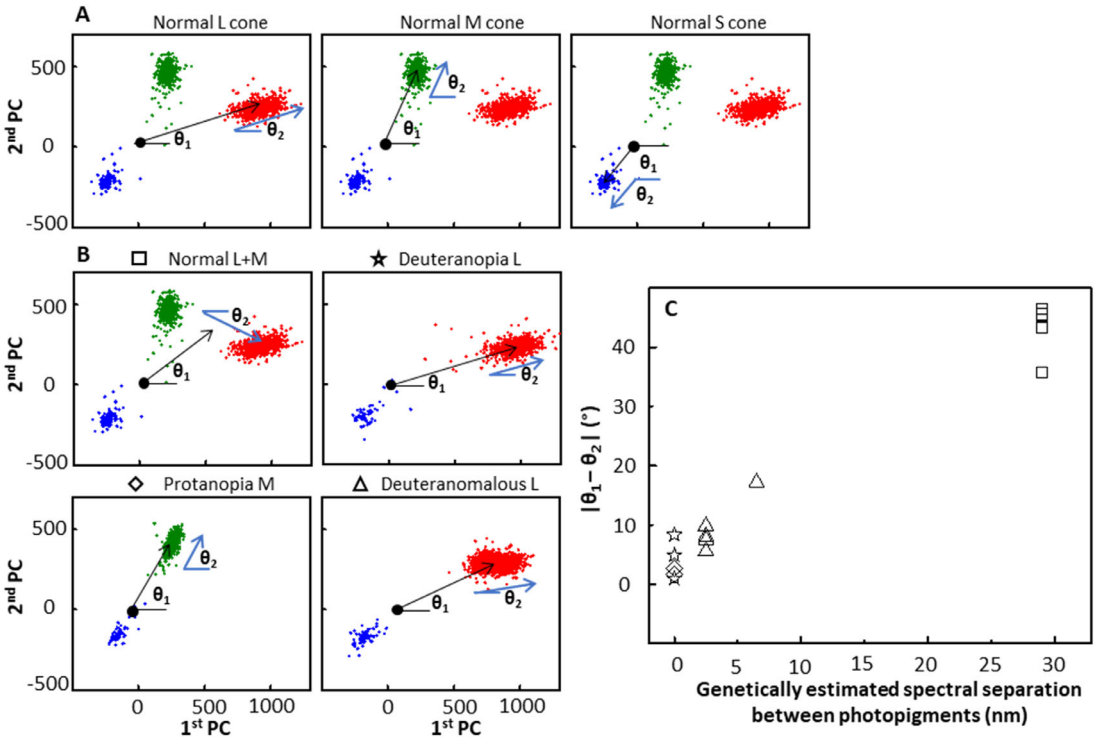

Figure 4. Differentiating color vision phenotype by cluster analysis in the PC space. (**A**) PC space plot illustrates the polar angle of the cluster centroid subtended at the origin (0,0), θ_1, and cluster orientation, θ_2 (along the dimension of maximum variance), of normal L (*left*), M (*middle*), and S (*right*) cones, respectively. The *black dot* is at coordinate (0,0) and corresponds to a cone that did not respond to any of the three stimuli. (**B**) θ_1 and θ_2 measurements of L + M cones in color-normal subjects, L cones in deuteranopes, M cones in protanopes, and L cones in deuteranomalous trichromats. (**C**) The relationship between cluster skewness ($|\theta_1$-$\theta_2|$) and genetic prediction of spectral separation (Table 1, rightmost column) in the same subjects. Phenotypes are labeled according to the symbols specified in **B**.

responses consistent with those of M and S cones with L cones absent. No L cluster was present in the PC space plots for subjects S9 and S10 in Figure 3.

Cone responses in the six deuteranomalous trichromats (subjects S11–S16) were similar to those of the three deuteranopes (subjects S6–S8), exhibiting responses consistent with L and S cones in the color-normal subjects and inconsistent with M cones (Fig. 3, PC space plots for subjects S11–S16). We know, however, that the genetics of deuteranopes and deuteranomalous trichromats are different, with the latter having two expressed L genes of slightly shifted peak absorptions, often designated as L_1 and L_2. This shift, by definition, must be present in our PC plots for the deuteranomalous subjects but is presumably masked by the relatively large spread of the L-cone cluster. Thus, we sought to determine whether analysis of individual cone clusters might reveal this additional information, a point we address next with the aid of Figure 4.

Detection of Cone Subtypes by Cluster Analysis

The position of each cone in the PC space is determined by its response to different wavelengths of light stimulus—in our study, 450 nm, 528 nm, and 637 nm. The cone response is governed by the intrinsic absorption properties of the cone (relative spectral sensitivity μ_λ and total number of photopigment molecules, p) and external stimulus energy E_λ. According to our experimental findings in the previous study,[15] we can express the influence of these on the ΔOPL_λ response as a power law:

$$\Delta OPL_\lambda = a \cdot (E_\lambda \cdot \mu_\lambda \cdot p)^b \quad (1)$$

where a and b are fitting constants. Of importance, cone spectral type, including L_1 and L_2 cones in deuteranomaly subjects, is determined solely by the relative spectral sensitivity μ_λ of the cone; thus, this parameter alone is what we seek to differentiate L_1 and L_2 cones. Unfortunately, although μ_λ is expected to be the same for cones of the same type, the photopigment population (p) is not.[27] Thus, cones of the same type will respond somewhat differently to the same stimulus. To complicate matters, a and b are also unknown. To remove the effects of p and a, we take the ratio of the response of the same cone at two different wavelengths of stimuli (λ_1 and λ_2):

$$\frac{\Delta OPL_{\lambda 1}}{\Delta OPL_{\lambda 2}} = \left(\frac{E_{\lambda 1}}{E_{\lambda 2}} \cdot \frac{\mu_{\lambda 1}}{\mu_{\lambda 2}}\right)^b \quad (2)$$

From Equation 2, we see that cones of the same spectral type must have the same response ratio ($\Delta OPL_{\lambda 1}/\Delta OPL_{\lambda 2}$) as they have the same μ_λ and are exposed to the same stimuli strength, E_λ. Therefore, cones of the same type must locate to a line in ($\Delta OPL_{\lambda 1}$, $\Delta OPL_{\lambda 2}$) space and, by definition then, a line when projected to the PC space. In both spaces, the line must intersect the origin (0,0), denoted by the black dots in the three examples of PC space in Figure 4A. For cone clusters in Figure 4A, the projected line is nominally

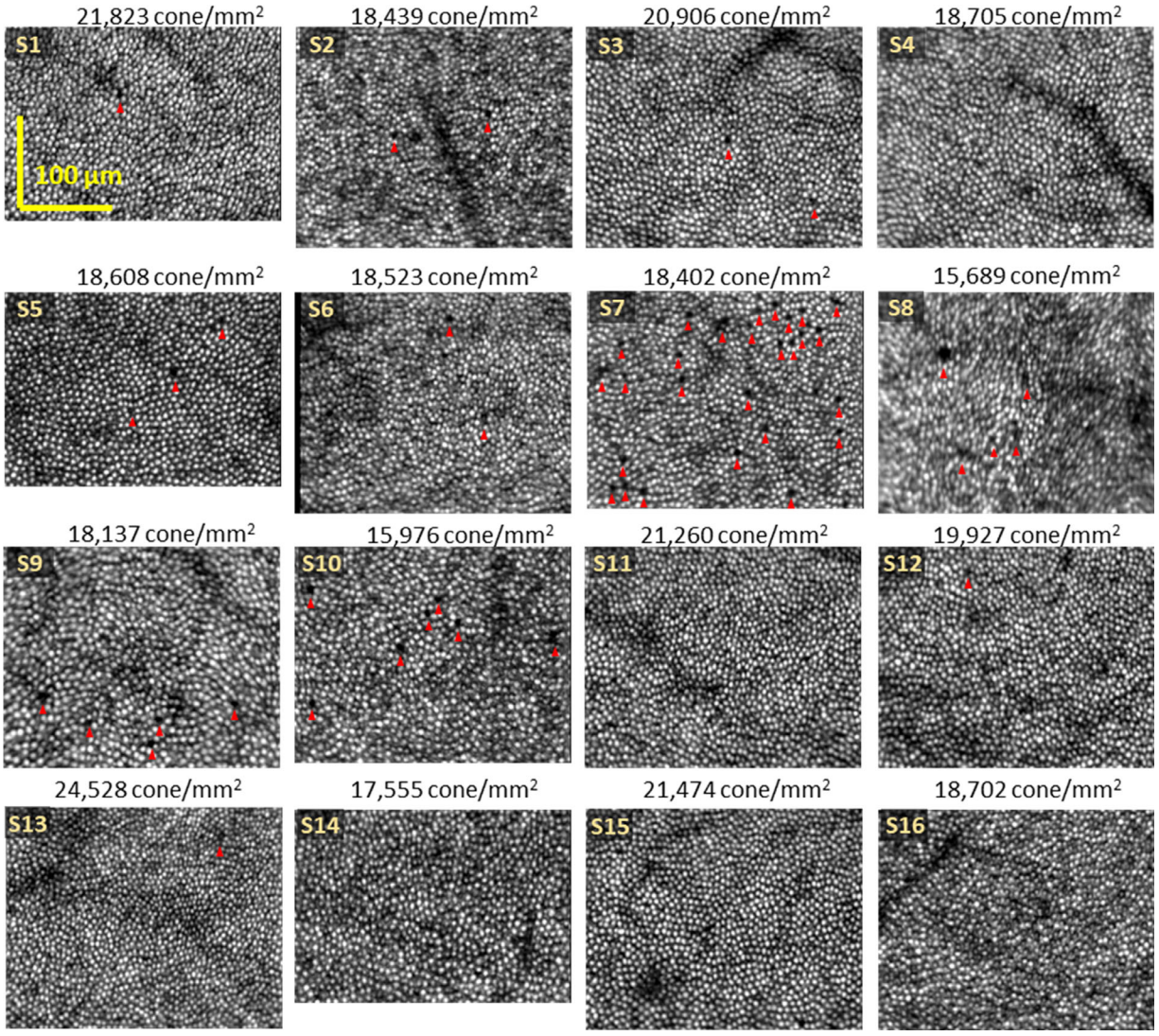

Figure 5. Cone mosaics segmented from the AO-OCT volumes that were acquired on all subjects. Cone density is given above each intensity image. *Red arrows* point to the most apparent dark holes; areas with vessel shadows were omitted.

the solid black line shown. We define the slope of this line by its polar angle, θ_1, subtended relative to the horizontal axis. Because of noise and measurement error, cones that would otherwise fall on this line are scattered, forming a cluster about the line. We therefore estimate θ_1 as the polar angle of the cluster centroid, which is located at one end of the black line in the examples shown in Figure 4A.

We also compute a second angle, θ_2, defined as the axis of maximum variance of the associated cluster (blue line in Fig. 4A plots). We use the absolute difference between these two angles ($|\theta_1–\theta_2|$) to quantify the degree of skewness of the cluster relative to the origin (0,0), with $|\theta_1–\theta_2| = 0$ corresponding to zero skewness; that is, the two lines defined by θ_1 and θ_2 are parallel.

In principle, clusters that contain only one type of cone will have θ_1 and θ_2 equal (zero skew), as shown by the examples in Figure 4A. Clusters with more than one type of cone (e.g., L_1 and L_2 for deuteranomalies) will have different θ_1 and θ_2 (skewed), as shown in Figure 4B. We substantiated this prediction by comparing skewness ($|\theta_1 - \theta_2|$) of each type of cone among the different phenotypes. The skewness values of the L cones of the normal, deuteranopic, and deuteranomalous subjects were 2.1° ± 1.8°, 4.7° ± 3.7°, and 9.3° ± 4.1°, respectively. A one-way ANOVA test with Bonferroni multiple comparison revealed no significant difference of L-cone skewness between normal and deuteranopic subjects ($P = 0.55$), but deuteranomalous subjects showed significantly higher skewness than normal subjects ($P = 0.01$). As expected, no significant difference was observed in the M-cone skewness between color-normal subjects (4.7° ± 4.0°) and protanopic subjects (2.2° ± 0.7°) ($P = 0.34$). Similarly, the S-cone cluster skewness values for the color-normal subjects, deuteranopes, protanopes, and deuteranomalous trichromats were 7.2° ± 10.4°, 8.3° ± 5.9°, 2.9° ± 4.0°, and 9.6° ± 7.8° respectively. The overall larger skewness and intersubject variance of S-cone clusters are likely due to reduced statistical power of the small population of S cones and the weaker response (signal) of S cones to the flash stimuli. Regardless, no significant difference was observed in the S-cone skewness among the four phenotypes ($P =$

Investigative Ophthalmology & Visual Science

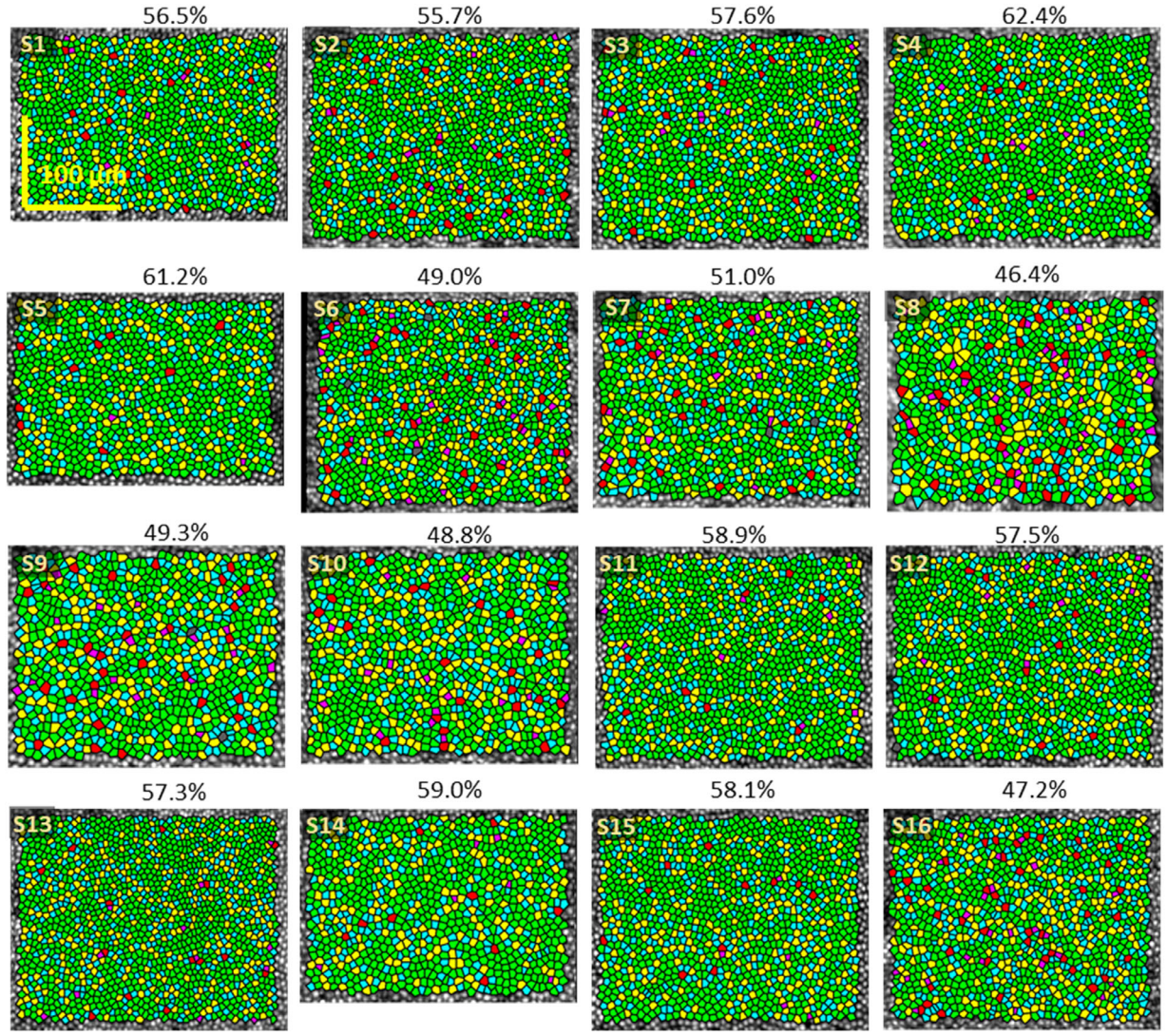

Figure 6. Cone mosaic arrangement assessed using Voronoi diagrams. Each cone is represented by a polygon that is color coded based on the number of neighboring cones: *magenta*, 4; *cyan*, 5; *green*, 6; *yellow*, 7; *red*, 8; and *gray*, >8. The number above each Voronoi diagram is the proportion of cones with six neighbors.

0.79). In conclusion, a significant increase in cluster skewness was observed only in L cones of the deuteranomalous subjects, thus pointing to the presence of multiple subtypes of L cones in this phenotype.

We next tested whether the severity of color vision deficiency as captured by our cone function measurements (i.e., our cluster skewness metric, $|\theta_1 - \theta_2|$), correlated with the predicted spectral separation of the first two opsin genes from the genetic test (Table 1, rightmost column) in the same subjects. Results are shown in Figure 4C. As is evident, skewness increased monotonically with predicted spectral separation, being largest (45.88° ± 4.22°) in the five color-normal subjects (M and L combined as one cluster) with a spectral separation of 29 nm between L and M cones and smallest (3.71° ± 2.97°) in the five dichromats with a spectral separation of 0 nm (either M or L cones present). In the four deuteranomalous trichromats with a predicted spectral separation of just 2.5 nm between the two heterozygous L pigments (S13–S16), θ_1 and θ_2 differed by 7.69° ± 1.77°. This difference more than doubled (increases to 17.16°) for S11, whose 6.5-nm spectral separation was the largest in our deuteranomalous subjects. Subject S12 was not included because the three L genes complicated the spectral separation estimation. In general, the strong correlation ($r = 0.98$, $P = 2.3\text{e-}11$) between cluster skewness and genetic spectral estimation suggests we have found a highly sensitive biomarker based on cone function that not only differentiates the major color vision phenotypes but also the severity of the deficiency within a phenotype.

Cone Mosaic Structure

In addition to measuring cone function, we analyzed the cone density and arrangement of the cone mosaic, which has been thought to provide further insight into the gene expression mechanism of cone opsins.[1] The cone mosaic and cone density of each subject are shown in Figure 5. High contrast cone mosaic images with minimum distortion were successfully obtained from all subjects, except for

Investigative Ophthalmology & Visual Science

S8, whose cone mosaic was significantly distorted and non-uniformly blurred. These image artifacts were likely caused by the notably larger eye motion of S8 compared to the other subjects. Nonetheless, even with these artifacts, individual cones could still be clearly delineated; thus, quantification of cone density and arrangement should have been minimally impacted. We adopted the Voronoi analysis to assess the arrangement of cone mosaics from similar studies that investigated how cone mosaics are affected by color vision deficiency.[28–32] In the Voronoi diagrams of cone mosaics shown in Figure 6, each cone is represented by a polygon color coded by number of neighbors. Normal cone mosaics are typically organized hexagonally, with each cone surrounded by six other cones, whereas disrupted mosaics may have altered percentages of cones with six neighbors.

For the five color-normal subjects, the cone density varied from 18,608 to 21,823 cones/mm^2 (average ± SD, 19,707 ± 1570 cones/mm^2), which agrees with other AO imaging reports at 3.7° temporal retina.[33,34] In the same subjects, the proportion of cones with six nearest neighbors (hexagonal arrangement in the Voronoi cone map) was 56.5% to 62.4% (average ± SD, 58.7% ± 3.0%), which is consistent with previous reports for normal cone mosaics.[28–31] From deuteranope S6, who carried a C203R mutated M gene, we measured a cone density of 18,523 cones/mm^2 and six-neighbor cone proportion of 49.0%. A z-score analysis (number of standard deviations from the normal mean) revealed no significant change of cone density ($P = 0.41$) but a significantly reduced percentage of six-sided cones ($P = 0.01$) in this subject. For the four single-gene dichromats S7 to S10, cone densities varied from 15,689 to 18,402 cones/mm^2 (average ± SD, 17,052 ± 1415 cones/mm^2), and six-neighbor cone proportion varied from 46.4% to 51% (average ± SD, 48.9% ± 1.9%). For the six deuteranomalous trichromats S11 to S16, we measured a cone density of 17,555 to 24,528 cones/mm^2 (average ± SD, 20,574 ± 2447 cones/mm^2) and six-neighbor cone proportions of 47.2% to 58.9% (average ± SD, 56.3% ± 4.5%). A one-way ANOVA with Bonferroni multiple comparison revealed no significant difference in the cone density between color-normal subjects S1 to S5 and single-gene dichromats S7 to S10 ($P = 0.15$), and color-normal subjects S1 to S5 and deuteranomalous trichromats S11 to S16 ($P = 0.75$). On the other hand, the single-gene dichromats S7 to S10 showed significantly altered cone arrangement in the mosaic ($P = 0.0035$), whereas deuteranomalous trichromats S11 to S16 showed no significant difference ($P = 0.53$).

In addition to quantifying cone density and cone mosaic arrangement, we qualitatively inspected the mosaics for dark holes, locations where cones were apparently absent. The most apparent holes are marked by red arrows in Figure 5. Although there was some ambiguity in differentiating missing cones from blood vessel shadows and selecting the most apparent holes, we generally observed more dark holes in the dichromat mosaics than in the color-normal and deuteranomalous mosaics.

Cone Proportion and Mapping the Chromatic Cone Mosaic

Using the cone classification results in Figure 3, we measured the proportion of each type of cone and mapped cone type to location to reconstruct the chromatic cone mosaic of each subject. Results are given in Table 2 and Figure 7. Note that some cones, mostly near the image edge, were not classified because eye motion resulted in insufficient averaging of AO-PSOCT images for these cones; these cells were identified by their noisier ΔOPL traces (root mean square > 30 nm prior to stimulation). These noisier traces are not indicative of non-responding cones, as a non-responding cone has no response (by definition) and thus cannot contribute to ΔOPL. Also, only about half of the cones of subject S8 were classified due to increased measurement noise caused by notably larger eye motion in this subject compared to the others. Nevertheless, it seems unlikely that eye motion would have a preference for cone class; therefore, the cone proportion we measured in the identified half should be a reasonable estimate of the total cone population.

Table 2. Proportions of Different Spectral Types of Cones in All Subjects As Determined Using AO-PSOCT

	Cone Proportion (%)		
Subject	**L**	**M**	**S**
S1	58.81	33.61	7.58
S2	55.35	39.65	5.00
S3	57.92	34.85	7.23
S4	45.78	46.79	7.43
S5	74.37	17.80	7.83
S6	91.7	0	8.3
S7	93.4	0	6.6
S8	91.65	0	8.35
S9	0	92.07	7.93
S10	0	91.90	8.10
S11	93.91	0	6.09
S12	92.25	0	7.75
S13	93.81	0	6.19
S14	90.82	0	9.18
S15	92.10	0	7.90
S16	90.14	0	9.86

As evident in Table 2, the S-cone proportion was generally similar across all 16 subjects at the 3.7° eccentricity location regardless of phenotype and ranged from 5.00% to 9.86% of the total cone population (average ± SD of 16 eyes, 7.58 ± 1.19%). This proportion agrees with histology[35] and retinal densitometry[11] at similar eccentricities. In contrast to the relatively stable S-cone proportion, the L/M ratio varied by more than fourfold among the color-normal subjects, ranging from 0.98 to 4.18 (average ± SD of five eyes, 1.99 ± 1.26).

Discussion

In this study, we used AO-PSOCT to measure the function of many thousands of cones in 16 human subjects with different phenotypes and genotypes of color vision. We found PCA to be an effective tool for analyzing our cone function results, reducing the 150 dimensions of our ΔOPL cone traces to just two dimensions. These two correspond to the first two principal components and capture most of the trace variance. In the PC space, cone types transform into clusters whose presence or absence, coordinate location, and degree of skewness were used as metrics to test against the subject's color vision phenotype and genotype. We used the same AO-PSOCT datasets to extract cone structural information (density, mosaic arrangement, prevalence of

Investigative Ophthalmology & Visual Science

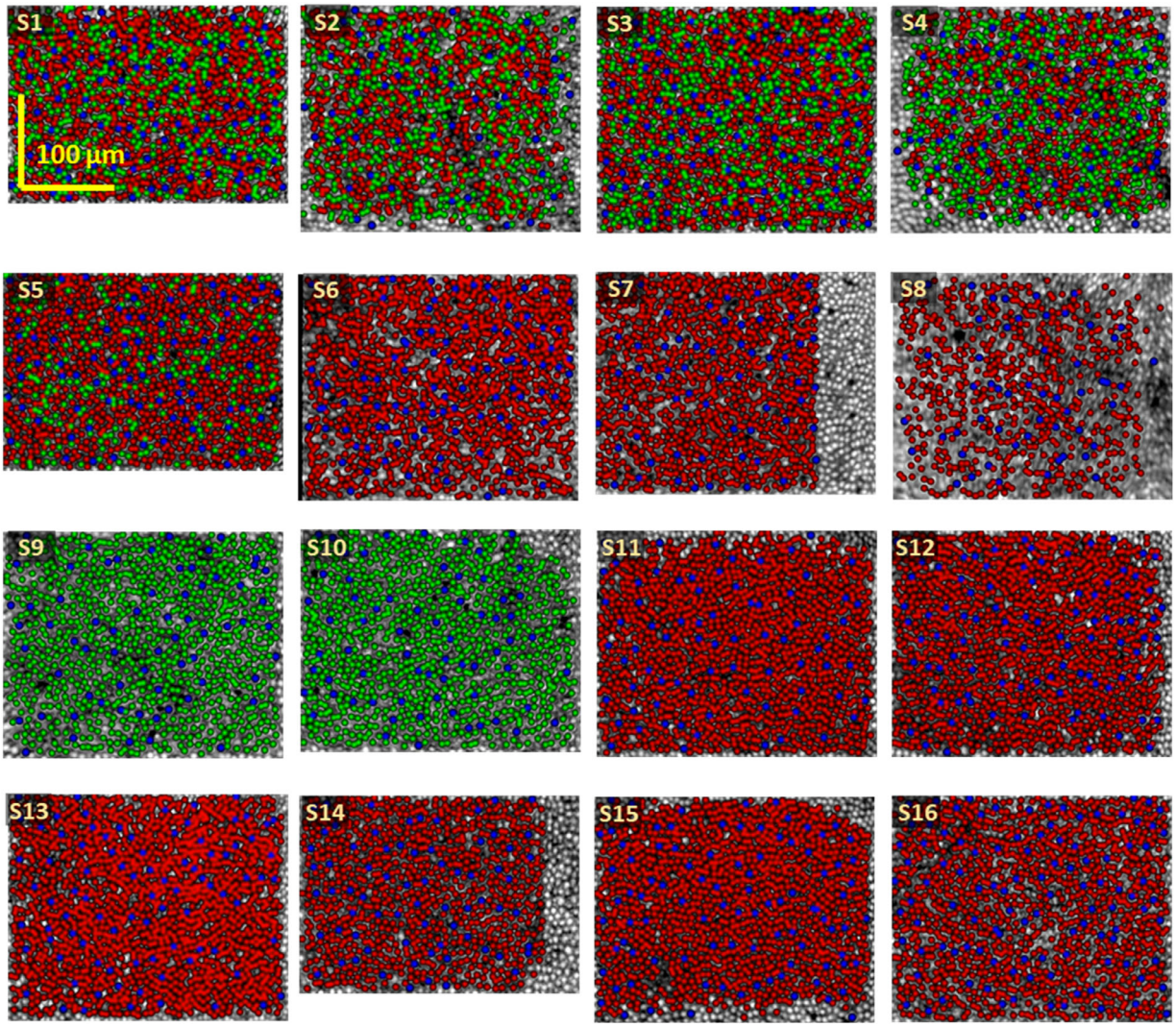

Figure 7. Chromatic cone mosaics of all subjects as determined using AO-PSOCT. Cones are color coded: *red* (L cone), *green* (M cone), and *blue* (S cone).

missing cones, and chromatic mosaic map) that we compared with the phenotype and genotype.

Color Vision Phenotype Manifested in Single Cone Cells

Our cone function results provide direct evidence that supports current understanding of how different phenotypes of color vision are embodied at the level of single cone cells. All of our color-normal subjects possessed three clearly distinct clusters of cone function (subjects S1–S5 in Fig. 3) in the PC space, with each cluster having a low degree of skewness. Low skewness supports the presence of only one subtype of cone per cluster. These findings support the trichromacy theory that normal color vision is realized by three spectral types of cones.[36] The centroid locations of the three clusters in polar coordinates (amplitude, angle) were similar among the subjects, with the L, M, and S cluster centroids being located at (903 ± 74, 14° ± 0.7°), (483 ± 47, 65.6° ± 1.3°), and (247 ± 47, –136° ± 2.1°), respectively.

In the PC plots of deuteranopes S6 and S7, the M-cone cluster is missing but the L- and S-cone clusters are present, with the L-cone cluster located at (989, 13.5°) for S6 and at (874, 17.5°) for S7 and the M-cone cluster located at (274, –132.3°) for S6 and at (210, –130.4°) for S7. Both fall within the centroid range of the L and S clusters of the color-normal subjects (reported above). Deuteranope S8 also showed no M-cone cluster, but his L-cone cluster had a higher degree of skewness (8.33°) than those of S6 and S7, indicative of multiple subtypes of L cones. We speculate that the discrepancy between our cone function measurement and the psychophysical and genetic testing (i.e., deuteranope vs. deuteranomalous trichromat) is likely attributed to the difficulty in imaging this subject due to his notably larger eye motion compared to the other subjects. For protanopes S9 and S10, the L-cone cluster was missing; the M and S cone clusters had a low degree of skewness and were located at (511 ± 33, 65° ± 9.8°) and (254 ± 44, –133.8° ± 1.8°), respectively, with both falling within the centroid range of the M- and S-cone clusters of the color-normal subjects (reported above). Collectively, our cone function results for the deuteranopes and protanopes support the hypothesis that

Investigative Ophthalmology & Visual Science

dichromatic color vision is a reduced form of trichromacy, where one type of cone is missing and the other two function like normal cones.[37]

Cluster distributions in the PC space of the deuteranomalous trichromats were highly similar to those of the deuteranopes (Fig. 3, compare S6–S8 to S11–S16). The M cluster was missing, and the L and S cluster centroids were located at (959 ± 119, 17.4° ± 1.3°) and (243 ± 36, –137.8° ± 2.9°), respectively. As we discovered, the L cluster exhibited an increased degree of skewness (triangle symbol in Fig. 4C), which could be explained by two or more slightly shifted, overlapping clusters, thus providing evidence of at least two subtypes of L cones. Our findings, therefore, support the hypothesis that deuteranomalous trichromats possess multiple subtypes of L cones.

This study was limited to four common phenotypes of color vision deficiency, but the ability of our method to measure cone function at the cellular level makes it readily applicable to study cone function in other phenotypes. These include tritanopia, protanomalous trichromacy, achromatopsia, and acquired color vision deficiencies. However, if these present with concomitant nystagmus (e.g., achromatopsia), our method is more challenging to apply due to (1) less frequent overlap of the AO-PSOCT images, and (2) a more degraded ΔOPL measurement of the cone cells. Reduced image overlap is an inherent limitation of all AO retinal imaging modalities, including AO flood illumination, AO scanning laser ophthalmoscopy (AO-SLO), and AO-OCT, due to their small field of view. We know that our measurement of the ΔOPL response of cone cells is sensitive to eye motion and thus will degrade in subjects with nystagmus, but to what extent remains to be determined.

Color Vision Genotype Expressed in Single Cone Cells

In dichromats, three different gene expression hypotheses have been proposed.[1] (1) The entire class of M cones in deuteranopia and entire class of L cones in protanopia are missing, resulting in substantial reduction of the total cone population. This reduction in cone number, however, may not necessarily result in a reduction in cone density at specific retinal locations, as cone migration during retinal development may mask regional cone loss. (2) M cones in deuteranopia and L cones in protanopia are present in the retina, but no photopigment gene is expressed in these cones, leading to their inability to function. (3) M cones in deuteranopia and L cones in protanopia are present in the retina, but they are filled with the pigment encoded by the remaining L or M gene: L gene in deuteranopia and M gene in protanopia.

In a previous AO-SLO study of five single-gene dichromats,[31] cone density and cone mosaic arrangement were found unaltered relative to those in color normals, thus supporting hypothesis 3. Our four single-gene dichromats, S7 to S10, were also found to have unaltered cone densities, but their cone mosaics arrangements were significantly different from those of the color-normal subjects, S1 to S5. Thus, our measurements on single-gene dichromats do not fit hypothesis 3 as completely as the previous study. Additionally, we found no evidence of non-functioning cones in our subjects (hypothesis 2), which would have appeared in the PC space at the origin (0,0). The absence of cones around the origin (0,0) is strikingly evident in the PC figures. Note, we fully expect our method to detect non-functioning cones that are anatomically intact even if they were to reflect less light or have compromised waveguiding. In a previous AO-PSOCT study, we found we could measure the phase (ΔOPL) of cones that were up to 25 times dimmer than the brightest neighboring cones.[15] Thus, we are able to measure function in cones whose reflectance spans a wide range.

Hypothesis 1 is more difficult to rule out. Although our single-gene dichromats showed no evidence of reduced cone density, any cone loss that might have occurred during retinal development could have been masked by subsequent cone migration, thus avoiding detection by our cone density measurements.

Consistent with the reduced percentage of six-sided cones, we observed more dark holes in the cone mosaics of single-gene dichromats (red arrows in Fig. 5). These dark holes are typically 25 to 45 times dimmer than their brightest neighboring cone and thus too dim to obtain a reliable ΔOPL measurement using our method. Dark patches have been found in dichromats with deleterious interchange mutations (e.g., LIAVA mutation),[14] but not in single-gene dichromats[12,31] or dichromats with missense mutations (e.g., C203R mutation)[32] that were studied here. The different findings in dark holes between our study and prior studies may be attributed to the different imaging modalities used: AO flood illumination,[31,32] AO-SLO,[12] and AO-OCT (this study). These dark holes could possibly be functional cones, as has been reported in both normal and diseased retinas, but they have not been associated with color vision deficiency.[38] Another possibility is that these dark holes represent cone loss. Interestingly, we found that the dark holes in our images are often associated with bright inner segment reflections (see movie S4 of Zhang et al.[15] for results of subject S7), suggesting that cones still retain their inner segment. This could be further substantiated with non-confocal AO-SLO imaging of the inner segment.[39] Alternatively, cone loss could be causally related to dichromacy in which the dark holes are a consequence of incomplete replacement of lost cones with cones of another type during retinal development, as suggested in hypothesis 1.

Deuteranope S6 had both L and M genes in his X-chromosome gene array, but the M gene carried the deleterious mutation C203R. As predicted, the mutated M gene was not expressed in the retina, as no M cone function was observed in this subject (subject S6 in Fig. 3). A previous study of two subjects with the C203R mutation on the photopigment gene revealed that the mutation can lead to a significantly lower cone density while retaining a normal cone mosaic arrangement, thus supporting hypothesis 1.[32] However, for our C203R subject, a *z*-score analysis (number of standard deviations from the normal mean) revealed no significant decrease of cone density ($P > 0.05$), and his cone mosaic had a significantly reduced proportion of six-sided cones ($P < 0.05$) compared to our color normals. Thus, this single example with the C203R mutation in our study does not fit the findings of the two subjects in the earlier study. The difference might be attributed to different onsets of cone degeneration during retinal development in these subjects. An earlier onset in our subject would have allowed greater cone migration into the macula and thus better masking of cone loss at the retinal locations measured in the two studies. In addition, the previous study did not find significantly lower cone densities at all retinal locations examined (two of five locations were not); thus, our single location might

Investigative Ophthalmology & Visual Science

simply be representative of these others. This requires more investigation.

It has long been argued whether genes beyond the second position in the X-chromosome gene array are expressed. Many studies[40–44] have hypothesized that only the first two genes are, as any additional ones are too distal from the locus control region located upstream of the array. However, an mRNA study[45] reported evidence that genes farther from the second position in the array can be expressed. Our ability to measure function of individual cone cells, as we have demonstrated here in deuteranomalous trichromats, may provide a direct means to test this controversy. As an example, although subjects S13, S15, and S16 had an extra M gene in the third position of their gene array, none of the more than 3000 cones that we examined in these subjects exhibited evidence of M-cone function (subjects S13, S15, and S16 in Fig. 3). Therefore, our functional results provide additional evidence supporting the hypothesis that only the first two photopigment genes in the gene array can be expressed.

As this example illustrates, our method can be readily used to test gene expression and is applicable to many of the different genotypes associated with color vision deficiency. The sensitivity and quantitative properties of our method may also make it attractive for assessing the outcome of gene therapies that have been developed recently to treat color vision deficiencies.[46] Moreover, it has been postulated that some females may possess more than three types of cones in their retina (tetrachromacy and pentachromacy), as they have two X-chromosomes that can potentially carry heterozygous L and M genes.[47] Our method provides a powerful tool to test this hypothesis.

Cone Proportions and Chromatic Cone Mosaic

Across all subjects, the S-cone proportion of the total cone population was relatively stable, ranging from 5.0% to 9.9%. We found no correlation of S-cone proportion with color vision phenotype and M and L genotype; thus, we concluded that S cones are likely independently expressed from L and M cones.

On the other hand, the five color-normal subjects with similar color matching performance and same genotype (Table 1) demonstrated strikingly different chromatic cone mosaics (Fig. 7) and high variability in their L/M cone ratios (range from 1.0 to 4.2 in Table 2). This observation is consistent with previously measured intersubject variability of L/M ratio,[10–12,20,48,49] confirming and extending the hypotheses that color perception in color-normal individuals is insensitive to the relative proportions of the L and M cones[11] and that the L/M ratio is independent of the photopigment genes themselves, which were identical across the five color-normal subjects.

AO-PSOCT As a Novel Method for Color Vision Assessment

Our AO-PSOCT-based method serves as a novel approach for elucidating the role cone photoreceptors play in color vision. In this study, we substantiated the ability of our method to discriminate cellular level functional and structural differences in different types and severities of color vision deficiency. This ability complements traditional psychophysical testing and recent genetic testing. Compared to psychophysics, which relies on subject feedback, our method is objective, and highly local, making it a natural tool for improving interpretation of psychophysical results, as we demonstrated in this study. It also has the ability to assess color vision in areas not readily applicable to psychophysics, such as in animal models.

Genetic testing has become a powerful clinical tool for color vision assessment and has established correlates with phenotype.[3] However, major gaps remain in our understanding of which genes are expressed, how they express themselves, and how mutations alter the expression in both associated and acquired color vision deficiencies. In contrast, our method is immune to these problems, as we directly detect cone function—the expression of whatever photopigment genes the subject has—and spatially resolve it across the retina.

There are also limitations of our method. First, the method relies on a complex optical system (AO-PSOCT) and processing algorithm that were custom developed in our laboratory and thus not available commercially. Nevertheless, we believe that with further maturation of AO-PSOCT and the general increased demand of high-resolution retinal imaging, our method has the potential to see broad scientific and clinical use. Second, the experiment in this study took 90 minutes to image each subject. Although too long for clinical use, the imaging protocol was not optimized for time. As we have shown previously, there is a tradeoff between experiment duration and cone classification accuracy.[15] We found that a single video acquired in 5 seconds (compared to the 15 videos acquired in 90 minutes in this study) can achieve a classification accuracy of 97%, which is sufficient to discriminate the deutan, protan, and tritan forms of color vision deficiency. Thus, there is a clear path for improvement in data acquisition to balance accuracy and efficiency to match application. Third, our method can successfully detect the presence of multiple subtypes of L (or M) cones in deuteranomalous (or protanomalous) trichromats. Although this success reflects a strength of our method, the fact that we can now detect these subtle spectral differences makes clear our inability to discriminate them. Note that our method has yet to be optimized for this task. Better discrimination of cone subtypes may be possible by optimizing the experimental protocol, such as, for example, by using other wavelengths of stimuli that maximize subtype differences, and by improving the data analysis, such as, for example, by including information from more than two PC components. These remain to be addressed in future work.

Conclusions

In this study, we elucidated how color vision genotype and phenotype manifest themselves in individual cone cells using AO-PSOCT and established AO-PSOCT as a novel method for color vision assessment.

Acknowledgments

The authors thank Jessica Rowlan at the University of Washington for performing the PCR and DNA sequencing and Stephen Burns and Arthur Bradley for helpful discussions about color vision.

Supported by grants from the National Eye Institute (R01-EY018339, R01 EY029808) and the University of Washington's

Vision Research Core (P30EY001730), and by an unrestricted grant from Research to Prevent Blindness.

Disclosure: **F. Zhang**, Indiana University (P); **K. Kurokawa**, Indiana University (P); **M.T. Bernucci**, None; **H.W. Jung**, None; **A. Lassoued**, None; **J.A. Crowell**, None; **J. Neitz**, None; **M. Neitz**, None; **D.T. Miller**, Indiana University (P)

References

1. Sharpe LT, Stockman A, Jägle H, Nathans J. Opsin genes, cone photopigments, color vision, and color blindness. In: Gegenfurtner KR, Sharpe LT , eds. *Color Vision: From Genes to Perception*. Cambridge, UK: Cambridge University Press; 1999:3–51.
2. Nathans J, Thomas D, Hogness DS. Molecular genetics of human color-vision: the genes encoding blue, green, and red pigments. *Science*. 1986;232(4747):193–202.
3. Davidoff C, Neitz M, Neitz J. Genetic testing as a new standard for clinical diagnosis of color vision deficiencies. *Transl Vis Sci Technol*. 2016;5(5):2.
4. Bowmaker JK, Dartnall HJA. Visual pigments of rods and cones in a human retina. *J Physiol*. 1980;298:501–511.
5. Schnapf JL, Kraft TW, Baylor DA. Spectral sensitivity of human cone photoreceptors. *Nature*. 1987;325(6103):439–441.
6. Mitchell D, Rushton W. Visual pigments in dichromats. *Vision Res*. 1971;11(10):1033–1043.
7. Rushton WA. A cone pigment in the protanope. *J Physiol*. 1963;168(2):345–359.
8. Neitz J, Jacobs GH. Electroretinogram measurements of cone spectral sensitivity in dichromatic monkeys. *J Opt Soc Am A*. 1984;1(12):1175–1180.
9. Liang JZ, Williams DR, Miller DT. Supernormal vision and high-resolution retinal imaging through adaptive optics. *J Opt Soc Am A Opt Image Sci Vis*. 1997;14(11):2884–2892.
10. Roorda A, Williams DR. The arrangement of the three cone classes in the living human eye. *Nature*. 1999;397(6719):520–522.
11. Hofer H, Carroll J, Neitz J, Neitz M, Williams DR. Organization of the human trichromatic cone mosaic. *J Neurosci*. 2005;25(42):9669–9679.
12. Sabesan R, Hofer H, Roorda A. Characterizing the human cone photoreceptor mosaic via dynamic photopigment densitometry. *PLoS One*. 2015;10(12):e0144891.
13. Roorda A, Metha AB, Lennie P, Williams DR. Packing arrangement of the three cone classes in primate retina. *Vision Res*. 2001;41(10-11):1291–1306.
14. Carroll J, Neitz M, Hofer H, Neitz J, Williams DR. Functional photoreceptor loss revealed with adaptive optics: an alternate cause of color blindness. *Proc Natl Acad Sci USA*. 2004;101(22):8461–8466.
15. Zhang F, Kurokawa K, Lassoued A, Crowell JA, Miller DT. Cone photoreceptor classification in the living human eye from photostimulation-induced phase dynamics. *Proc Natl Acad Sci USA*. 2019;116(16):7951–7956.
16. Hillmann D, Spahr H, Pfaffle C, Sudkamp H, Franke G, Huttmann G. In vivo optical imaging of physiological responses to photostimulation in human photoreceptors. *Proc Natl Acad Sci USA*. 2016;113(46):13138–13143.
17. Azimipour M, Migacz JV, Zawadzki RJ, Werner JS, Jonnal RS. Functional retinal imaging using adaptive optics swept-source OCT at 1.6 MHz. *Optica*. 2019;6(3):300–303.
18. Pandiyan VP, Maloney-Bertelli A, Kuchenbecker JA, et al. The optoretinogram reveals the primary steps of phototransduction in the living human eye. *Sci Adv*. 2020;6(37):eabc1124.
19. Bennett AG, Rudnicka AR, Edgar DF. Improvements on Littmann method of determining the size of retinal features by fundus photography. *Graefes Arch Clin Exp Ophthalmol*. 1994;232(6):361–367.
20. Carroll J, Neitz J, Neitz M. Estimates of L:M cone ratio from ERG flicker photometry and genetics. *J Vis*. 2002;2(8):531–542.
21. Liu ZL, Kocaoglu OP, Miller DT. In-the-plane design of an off-axis ophthalmic adaptive optics system using toroidal mirrors. *Biomed Opt Express*. 2013;4(12):3007–3029.
22. Kocaoglu OP, Turner TL, Liu ZL, Miller DT. Adaptive optics optical coherence tomography at 1 MHz. *Biomed Opt Express*. 2014;5(12):4186–4200.
23. Laser Institute of America. *ANSI Z136.1 A. American National Standard for Safe Use of Lasers*. Orlando, FL: Laser Institute of America; 2014.
24. Rushton WA, Henry GH. Bleaching and regeneration of cone pigments in man. *Vision Res*. 1968;8(6):617–631.
25. Hotelling H. Analysis of a complex of statistical variables into principal components. *J Educ Psychol*. 1933;24(6):417–441.
26. MacQueen J. Some methods for classification and analysis of multivariate observations. In: Le Cam LM, Neyman J , eds. *Proceedings of the Fifth Berkeley Symposium on Mathematical Statistics and Probability*. Berkeley, CA: University of California Press; 1967:281–297.
27. Bedggood P, Metha A. Optical imaging of human cone photoreceptors directly following the capture of light. *PLoS One*. 2013;8(11):e79251.
28. Baraas RC, Carroll J, Gunther KL, et al. Adaptive optics retinal imaging reveals S-cone dystrophy in tritan color-vision deficiency. *J Opt Soc Am A Opt Image Sci Vis*. 2007;24(5):1438–1447.
29. Li KY, Roorda A. Automated identification of cone photoreceptors in adaptive optics retinal images. *J Opt Soc Am A Opt Image Sci Vis*. 2007;24(5):1358–1363.
30. Carroll J, Rossi EA, Porter J, et al. Deletion of the X-linked opsin gene array locus control region (LCR) results in disruption of the cone mosaic. *Vision Res*. 2010;50(19):1989–1999.
31. Wagner-Schuman M, Neitz J, Rha J, Williams DR, Neitz M, Carroll J. Color-deficient cone mosaics associated with Xq28 opsin mutations: a stop codon versus gene deletions. *Vision Res*. 2010;50(23):2396–2402.
32. Carroll J, Baraas RC, Wagner-Schuman M, et al. Cone photoreceptor mosaic disruption associated with Cys203Arg mutation in the M-cone opsin. *Proc Natl Acad Sci USA*. 2009;106(49):20948–20953.
33. Chui TYP, Song HX, Burns SA. Adaptive-optics imaging of human cone photoreceptor distribution. *J Opt Soc Am A Opt Image Sci Vis*. 2008;25(12):3021–3029.
34. Song H, Chui TY, Zhong Z, Elsner AE, Burns SA. Variation of cone photoreceptor packing density with retinal eccentricity and age. *Invest Ophthalmol Vis Sci*. 2011;52(10):7376–7384.
35. Curcio CA, Allen KA, Sloan KR, et al. Distribution and morphology of human cone photoreceptors stained with anti-blue opsin. *J Comp Neurol*. 1991;312(10):610–624.
36. Young T. The Bakerian Lecture: on the theory of light and colours. *Philos Trans R Soc Lond*. 1802;92:12–48.
37. König A, Dieterici K. Die Grundempfindungen in normalen und anormalen Farbensystemen und ihre Intersitätsverteilung in Spektrum. *Z Psychol Physiol Sinnesorg*. 1893:241–347.
38. Tu JH, Foote KG, Lujan BJ, et al. Dysflective cones: visual function and cone reflectivity in long-term follow-up of acute bilateral foveolitis. *Am J Ophthalmol Case Rep*. 2017;7:14–19.

39. Patterson EJ, Kalitzeos A, Kasilian M, et al. Residual cone structure in patients with X-linked cone opsin mutations. *Invest Ophthalmol Vis Sci*. 2018;59(10):4238–4248.
40. Winderickx J, Battisti L, Motulsky AG, Deeb SS. Selective expression of human X-chromosome-linked green opsin genes. *Proc Natl Acad Sci USA*. 1992;89(20):9710–9714.
41. Yamaguchi T, Motulsky AG, Deeb SS. Visual pigment gene structure and expression in human retinae. *Hum Mol Genet*. 1997;6(7):981–990.
42. Hayashi T, Motulsky AG, Deeb SS. Position of a 'green-red' hybrid gene in the visual pigment array determines colour-vision phenotype. *Nat Genet*. 1999;22(1):90–93.
43. Bollinger K, Sjoberg SA, Neitz M, Neitz J. Topographical cone photopigment in deutan-type red-green color gene expression vision defects. *Vision Res*. 2004;44(2):135–145.
44. Neitz M, Bollinger KE, Neitz J. Middle wavelength sensitive photopigment gene expression is absent in deuteranomalous colour vision. In: Mollon JD, Knoblauch K Pokorny J, eds. *Normal and Defective Colour Vision*. Oxford, UK: Oxford University Press; 2010:318–327.
45. Sjoberg SA, Neitz M, Balding SD, Neitz J. L-cone pigment genes expressed in normal colour vision. *Vision Res*. 1998;38(21):3213–3219.
46. Mancuso K, Hauswirth WW, Li QH, et al. Gene therapy for red-green colour blindness in adult primates. *Nature*. 2009;461(7265):784–787.
47. Neitz J, Neitz M. The genetics of normal and defective color vision. *Vision Res*. 2011;51(7):633–651.
48. Carroll J, McMahon C, Neitz M, Neitz J. Flicker-photometric electroretinogram estimates of L:M cone photoreceptor ratio in men with photopigment spectra derived from genetics. *J Opt Soc Am A Opt Image Sci Vis*. 2000;17(3):499–509.
49. Kremers J, Scholl HP, Knau H, Berendschot TT, Usui T, Sharpe LT. L/M cone ratios in human trichromats assessed by psychophysics, electroretinography, and retinal densitometry. *J Opt Soc Am A Opt Image Sci Vis*. 2000;17(3):517–526.

Investigative Ophthalmology & Visual Science